16th World Conference on Earthquake Engineering, 16WCEE 2017
Santiago Chile, January 9th to 13th 2017
Paper N° 4567
Registration Code: S-XXXXXXXX

RAPID DAMAGE DETECTION FROM STRONG MOTION ACCELERATION AND ROTATION RESPONSE MEASUREMENTS

Y. Liao[(1)], K. Balafas[(2)], A. Kiremidjian[(3)], R. Rajagopal[(4)], C. Loh[(5)]
[(1)] *PhD student, Department of Civil and Environmental Engineering, Stanford University, USA, yzliao@stanford.edu*
[(2)] *PhD student, Department of Civil and Environmental Engineering, Stanford University, USA, balafas@stanford.edu*
[(3)] *Professor, Department of Civil and Environmental Engineering, Stanford University, USA, ask@stanford.edu*
[(4)] *Assistant Professor, Department of Civil and Environmental Engineering, Stanford University, USA, ramr@stanford.edu*
[(5)] *Professor, Department of Civil Engineering, National Taiwan University, Taiwan, lohc0220@ntu.edu.tw*

Abstract

Assessment of various levels of damage severity immediately after a large earthquake is imperative for rapid recovery of the affected region. Recent research on the use of 3D strong motion acceleration and 3D gyroscope measurements has shown that sufficiently reliable rotations can be obtained along the height of a structure. By fitting a polynomial through these rotation values, the deformed shape of a structure can be estimated. The model for deformation estimates is compared to direct displacement measurements of simulations and laboratory experiment. The results show very good comparison between the estimated and measurement displacements. Correlation of these displacements to rapid warnings of green, yellow and red levels of risk can be very important in emergency response, especially when there is a high likelihood of collapse.

Keywords: Structural health monitoring; Accelerometer; Gyroscope; Displacement Estimation; Residual Displacement

1. Introduction

During past several decades, structural health monitoring (SHM) systems have been proved to give quick evaluation of structural damage after earthquakes and other extreme events. Since many civil infrastructures, such as bridges and buildings, are exposed to complex loadings and environment, it is necessary to continuously monitor the performance level and safety of structures during daily operation and extreme events like earthquakes and hurricanes.

In SHM, the structural displacement is one of the simple indicators of potential damage. Correlation of these displacements to rapid warnings of green, yellow and red levels of risk can be very important in emergency response, especially when there is a high likelihood of collapse. However, in many applications, the direct displacement measurements are hard to obtain. For example, the authors in [1] use global position systems (GPS) to measure the displacement of a tall building. GPS requires a direct connection with satellites and have limited performance if the sensor is installed indoor. In [2], draw-wire sensors are employed to measure the longitudinal displacements of a bridge. This type of sensors requires cable connection and power supply, which are unavailable in many filed applications. Also, the cost of the data acquisition system is high. These limitations make the displacement measurements difficult to obtain in the field or after earthquakes.

Recently, with the development of sensing technology, many new low-cost microelectromechanical sensors (MEMS) become available. These sensors provide many new structural quantities, which are not available or expensive to measure before. Recent research works have demonstrated that these newly available information could improve the reliability and accuracy of structural damage detection [3, 4]. For example, many off-the-shelf sensors have both accelerometers and gyroscopes on board now. They are synchronized and provide measurements simultaneously. Therefore, we can use both signals to estimate the dynamic and residual displacements.

This paper presents a displacement estimation algorithm of civil structures, which uses the three dimensional acceleration and rotation measurements to estimate both dynamic displacement and residual displacement drift. The algorithm is derived for single-column structures and then extended to multi-story structures. We use an experimental data set to validate the performances of the proposed algorithms.

2. Dynamic Displacement Estimation Using Accelerometer and Gyroscope

Dynamic displacement estimation requires measurements to be taken from structural columns. If we can determine the rotation at sensor location, it will be possible to solve displacements at other locations along the column. For example, in Fig. 1, a column is fixed at one end and has free vibration at the other end. Also, we assume the plastic rotation in a column is concentrated at a plastic hinge location at the base of the column and rest remains elastic. In Fig. 1, a sensor is installed at the height of h. If the column only vibrates along x-axis, the displacement D at the height H has following relationship:

$$d/h=D/H=\tan(\theta) \tag{1}$$

where θ is the sensor rotation angle. Usually h and H are known. If the rotation angle θ can be estimated, the displacement D can be uniquely determined. To improve the estimation accuracy, we can install multiple sensors at various locations along the column, and use linear regression to compute D. Given M sensors on a column, each sensor has a measurement of θ. Then, at each sensor's location, we can compute h and d. At last, we can use local h and d to fit a linear regression, i.e.

$$d = \beta_0 + \beta_1 h. \tag{2}$$

Once β_0 and β_1 are estimated, we can determine the displacement D as $D = \beta_0 + \beta_1 H$.

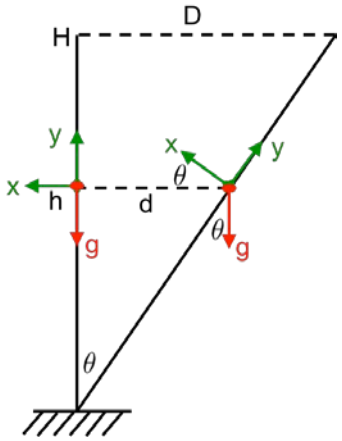

Fig.1 – Illustration of sensor rotation. h is the height of sensor; H is the floor height; d is the sensor displacement; and D is the floor displacement.

Gyroscope is a sensor that measures the angular velocity ω. Therefore, if we install one or more gyroscopes along a column, we can measure the rotation angle θ and the column displacement in real-time. The rotation angle $\theta[n]$ at a discrete time n can be computed as

$$\theta[n] = \theta[n-1] + \omega[n]\Delta T, \tag{3}$$

where ΔT denotes the sampling rate and $\omega[n]$ denotes the angular velocity at time n.

Sensor measurements usually are noisy. Over a long period of operation, the errors introduced by the gyroscope response $\omega[n]$ will be accumulated, and the rotation angle $\theta[n]$ will have an offset. This phenomenon is called sensor drift. A common way to reduce the effect of drift is using both gyroscope and accelerometer measurements. As shown in Fig. 1, if the sensor has an accelerometer, we can estimate the rotation angle using the acceleration measurements along x- and y-axis, i.e.,

$$\theta_a[n] = \arctan\left(\frac{a_x[n]}{a_y[n]}\right), \tag{4}$$

where $a_x[n]$ and $a_y[n]$ denote the acceleration response of x- and y-axis at time n respectively. The acceleration signals are sensitive to vibration and produce a noisy esitmation of rotation angle. In order to overcome the drift introduced by the gyroscope and the estimation noise introduced by the accelerometer, we use the complementary filter, which is defined as

$$\theta[n] = \alpha(\theta[n-1] + \omega[n]\Delta T) + (1-\alpha)\theta_a[n], \tag{5}$$

where α is the regularization parameter. When $\alpha = 0$, Equation (5) becomes to Equation (4). When $\alpha = 1$, Equation (5) becomes to Equation (3). In the complementary filter, the gyroscope signals are filtered by a high-pass filter, which removes the drift. The acceleration signals are filtered by a low-pass filter, which removes the vibration noise. Once the rotation angle $\theta[n]$ is obtained, we can estimate the displacement using Equations (1) and (2). The algorithm is summarized in Fig. 2.

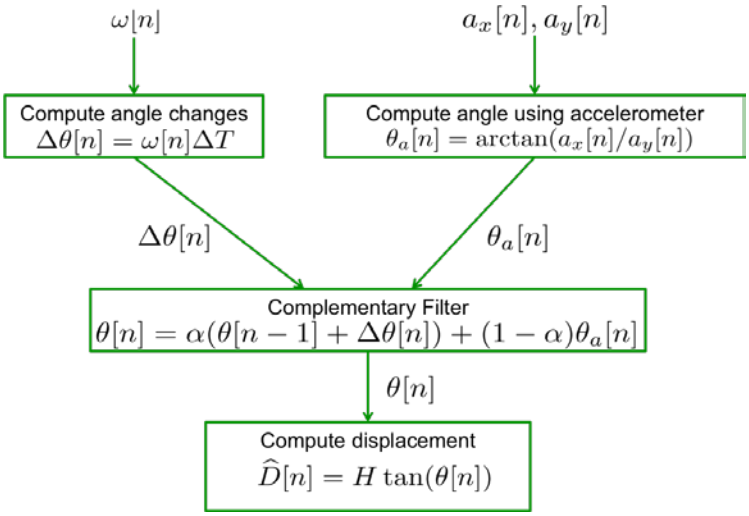

Fig. 2 --- Flow chart of the proposed dynamic displacement estimation method

The calculation of the rotation measurements can be embedded on the microprocessor of sensing units, thus requiring the transmission of only the final rotation values. While the estimation of displacements requires the rotations from more than one sensors, the calculations involved can also be embedded on the microprocessor of the base station, which can then report the estimated displacements directly to the end user. Thus, the proposed algorithm provides a computationally efficient method to obtain reliable information on the dynamic displacements of a structure almost immediately after an extreme loading event.

3. Residual Displacement Estimation Using Acceleration Measurements

In some diagnosis systems, we are more interested in the drift of structures after an earthquake. To estimate the residual displacement caused by an earthquak, we can still use the algorithm in Fig. 2 with simple modifications. This residual displacement estimation algorithm is developed on the premise that ambient vibrations are measured before and immediately after an earthquake. These measurements are then used to compute the rotation of the column at the location of the sensor. The residual displacement of the column is estimated by calculating the length of the plastic hinge region based on [5] and assuming that all of the rotations are concentrated at mid-height of the hinge.

Some recent studies, such as [6], have shown that the estimator in [5] may underestimate the true plastic hinge length, which leads to the overestimate of the residual displacement obtained from the algorithm in [7]. For this reason, in [8], the authors extend the rotation algorithm to use the recordings of multiple sensors. Multiple sensors along the height of the structure are selected and the rotations at the sensor locations are computed before and immediately after an earthquake based on the ambient vibration measurements. Let a_x and a_z denote the acceleration measurements along the shaking direction and along the gravity direction respectively. If the structure is symmetric, the rotation θ can be estimated using the same methodology as Equation (4):

$$\hat{\theta} = \arctan\left(\frac{a_x^{after}}{a_z^{after}}\right) - \arctan\left(\frac{a_x^{before}}{a_z^{before}}\right), \quad (6)$$

where a_x^{before} refers to the acceleration before earthquake and a_x^{after} refers to the acceleration after earthquake. Then, the rotations estimated at each sensor location are fitted with a polynomial function. For example, if the rotation estimates are fitted with a forth order polynomial function, we have

$$\hat{\theta} = \beta_1 h^4 + \beta_2 h^3 + \beta_3 h^2 + \beta_4 h + \beta_5, \quad (7)$$

where h denotes the height of the sensor above ground. After that, the fitted polynomial function is integrated with respect to the structural height to provide a function that estimates the residual displacement R, as shown below:

$$\hat{R} = \int (\hat{\beta}_1 h^4 + \hat{\beta}_2 h^3 + \hat{\beta}_3 h^2 + \hat{\beta}_4 Hh + \hat{\beta}_5) dh \quad (8)$$

$$= \frac{\hat{\beta}_1}{5} h^5 + \frac{\hat{\beta}_2}{4} h^4 + \frac{\hat{\beta}_3}{3} h^3 + \frac{\hat{\beta}_4}{2} h^2 + \hat{\beta}_5 h \quad (9)$$

Since the structure base is assumed to be fixed, we assume that there is no displacement at the base. Hence, the intercept term is zero and is ignored in Equation (9). Similarly, the residual displacement esitmation method can be embedded on the wireless senosrs and base station. This advantage allows us to obtain the residual displacement immendiately after any extreme event.

4. Algorithm Validation

4.1 Description of Experiment

This experiment was designed and performed at NCREE. Two identical three story single bay steel frames were constructed. Both structures have an inter story height of 1.1 meters. Floor dimension at every story is 1.1 meters by 1.5 meters. The columns have rectangular cross-sections with a dimension of 0.15 meters by 0.025 meters by 1.06 meters. As indicated in Fig 3, for Specimen 2, the NW column is replaced with a weakened column, which has a thickness of 0.015 meters. Thus, Specimen 1 is a symmetric structure while Specimen 2 is non-symmetric. In this section, we only focus on Specimen 1.

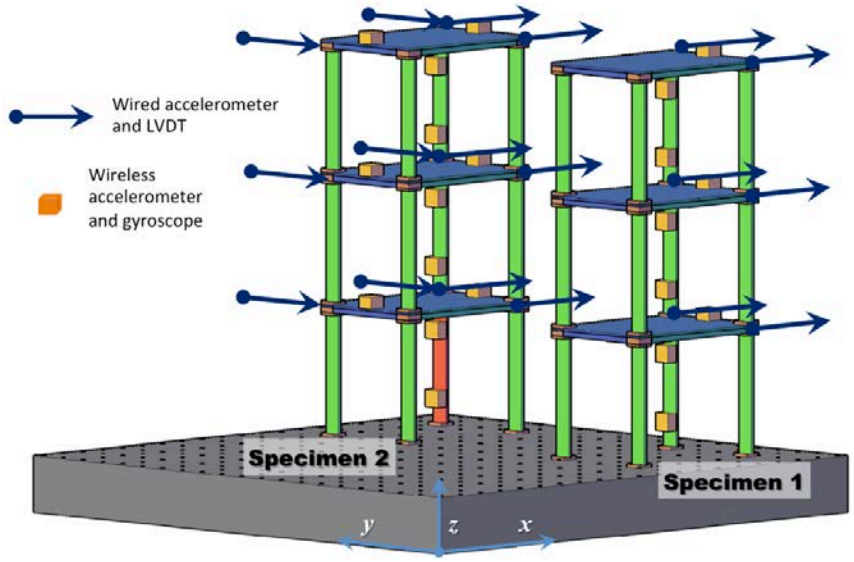

Fig. 3 -- Two structures and sensor locations used at the NCREE experiment. The weakened column is in red.

These two structures were placed side by side on the same shake table. The record of the 1999 Chi-Chi earthquake Station TCU 071 was used as the base excitation of the experiment. The excitation was applied in the x-direction with amplitudes progressively increasing from 100 to 1450 gals. Fig. 4 shows an example of the earthquake signal with a peak of 1000 gal. The earthquake amplitudes are summarized in Table. 1. The achieved amplitudes are the peaks of the vibration measured by the shake table.

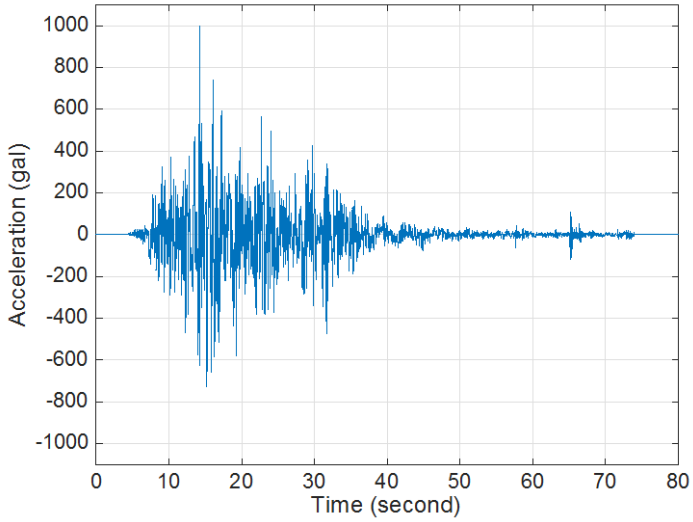

Fig. 4 – Earthquake signal of 1999 Chi-Chi earthquake. The signal was collected at Station TCU 071 and was scaled to have a peak of 1000 gals.

Table 1 – Summary of Ground Motions

Run Number	Desired Amplitude (gals)	Achieved Amplitude (gals)
1	100	95
2	250	269
3	400	400
4	550	572
5	700	674
6	850	858
7	1000	994
8	1150	1190

In this experiment, both wired and wireless sensors were installed for data acquisition, as shown in Fig. 3. All the analog sensors were connected with a common Analog-to-Digital Converter (ADC) with a sampling frequency of 200 Hz. The cut-off frequency of the anti-aliasing filter was 50 Hz. Each wireless sensing device was assembled with a Telosb mote [9, 10] and a 16-bit digital sensor, including a three-axis accelerometer and a three-axis gyroscope [11]. These motes were operating within the SnowFort system, an open source wireless sensor system designed for infrastructure monitoring [12]. The data were collected at 51.2 Hz sampling frequency and filtered with a 20 Hz anti-aliasing filter. The sampling frequency is fractional because the onboard microprocessor used 1024 ticks to represent one second and we set the mote to sample every 20 ticks. The wireless accelerometers had a measurement range of +/- 2g. The sensitivity was 16384 least significant bits (LSB) per g. The gyroscopes had a range of +/- 250 degrees per second (deg/sec) with a sensitivity of 131 LSB per deg/sec. According to [11], the accelerator has an average noise level of 1.265 mg and the gyroscope has an average noise level of 0.016 deg/sec.

4.2 Experimental Results of Dynamic Displacement Estimation

Fig. 5 shows the rotation angle estimation by using the complementary filter (Eq. (5)), accelerometer (Eq. (4)), and gyroscope (Eq. (3)) respectively. As shown in Fig. 3, the sensors were installed on the columns. We can see that the estimated angles using the acceleration responses are very noisy and have large amplitude. Also, the estimated angles using the gyroscopes have a clear offset over time. The complementary filter combines both signals and produces a smooth signal without any offset.

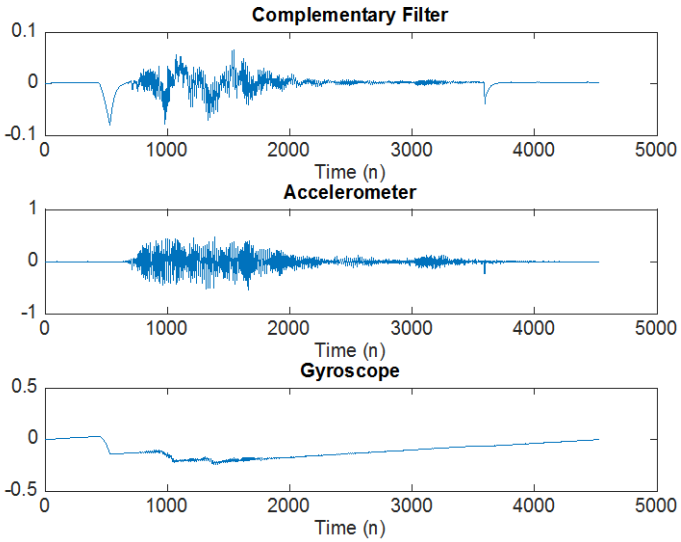

Fig. 5 -- Rotation angle ($\theta[n]$) estimation of Specimen 1 Floor 1 during Run 5 by the complementary filter, accelerometer, and gyroscope.

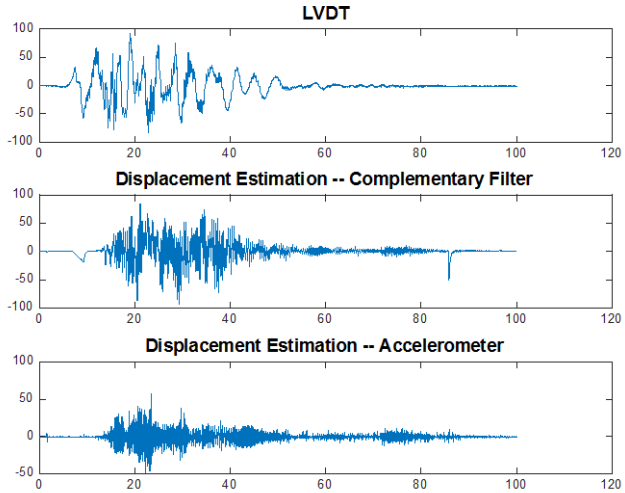

Fig 6 – Displacement (D) measured by LVDT and estimated by complementary filter and accelerometer of Specimen 1 Floor 1 during Run 5. The unit is mm.

Fig. 6 shows the displacements measured by LVDT and estimated by the complementary filter and accelerometer. The sensors are installed at columns and the displacements are measured and estimated at floor heights. The LVDT signals were preprocessed and filtered by a low-pass filter. Therefore, this signal looks very smooth. The displacement estimated by the complementary filter uses the two sensors on the column. In Fig. 6,

the envelope of estimated displacement is similar to that of the directed measurements from LVDT. Also, the peaks of the direct measurement and estimated displacement are very similar. In Fig. 6, we also illustrate the displacement estimated by integrating the acceleration signal twice. Clearly, the estimated displacement is noisier than the estimation based on the complimentary filters. Also, the estimated peak is much smaller than the peak obtained by LVDT.

Table 2 shows the peak displacements of direct measured and estimated displacements. From Table 2, we can observe that the peak of the estimated displacement by the complementary filter is closer to the true displacement measured by the LVDT. In addition, as the amplitude of ground motion increases, the difference between the directly measured peak and the estimated peak becomes smaller. For example, during Run 1, the difference is about 6mm. During Run 6, the difference is reduced to less than 1mm. This is observation is due to the sensor noise and resolution. When the amplitude of ground motion is low, the signal-to-noise ratio of sensor measurement is low. Therefore, the displacement estimation is far way from the true measurement. When the ground motion becomes strong, the signal-to-noise ratio becomes larger and the estimation method has better performance.

Table 2 -- Peak displacement of Specimen 1 Floor 1.

Run	LVDT (mm)	Complementary Filter (mm)	Accelerometer (mm)
1	14.8653	20.8089	22.4400
2	41.7862	45.0247	47.8257
3	59.5295	60.9200	62.9520
4	79.9475	81.1538	85.0782
5	92.4409	93.8918	114.8937
6	117.3312	116.5927	163.7939
7	126.4404	128.4456	145.4661

4.3 Experimental Results of Residual Displacement Estimation

In order to estimate the displacements, the measurements collected by the wireless sensors installed on the columns are selected. As we have discussed previously, the story height is H = 1.1m. All sensors in the same specimen are utilized and a fourth order polynomial is used to estimate the residual displacements R. The rotations at the sensor locations are calculated using 500 points (approximately 10 seconds) of ambient vibration before and after each ground motion.

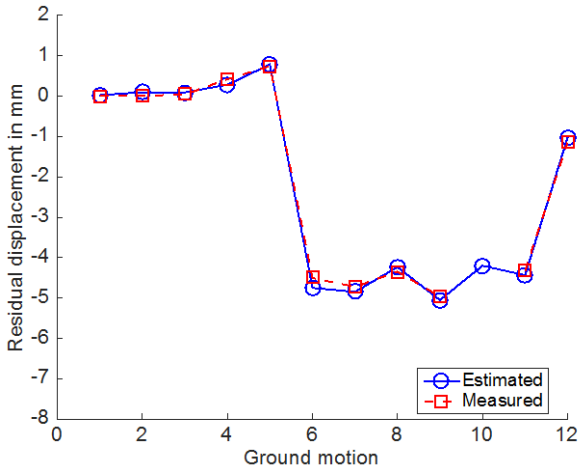

Fig. 7 – Estimated and measured residual displacements for Specimen 1 Floor 1 in the shaking direction (x-axis)

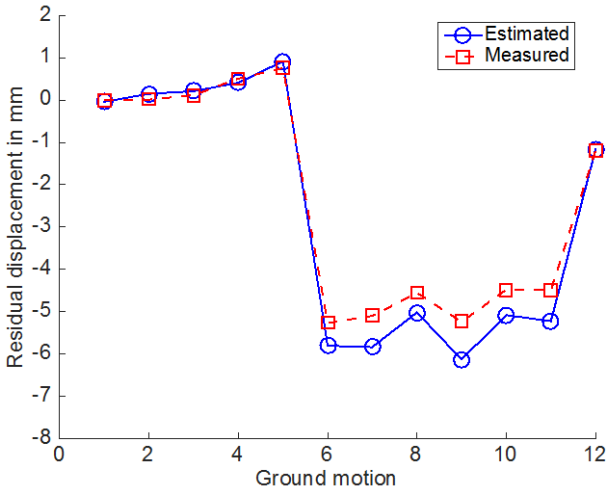

Fig. 8 -- Estimated and measured residual displacements for Specimen 1 Floor 2 in the shaking direction (x-axis)

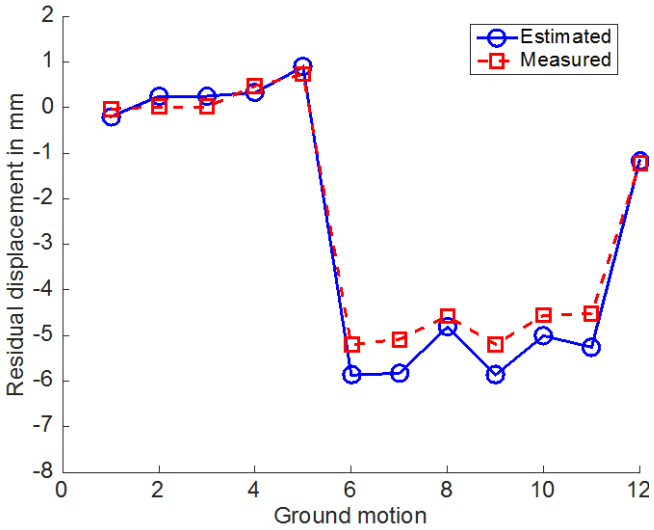

Fig. 9 --- Estimated and measured residual displacements for Specimen 1 Floor 3 in the shaking direction (x-axis)

Fig. 7 – 9 show a comparison between the estimated displacements and direct displacement measurements obtained through LVDTs. It should be noted that the rotations were measured and computed at the locations of the wireless sensors (two per story). But the displacements reported in Fig. 7 - 9, which are estimated by using Equation (9), are at the floor heights, where LVDTs were installed. This highlights the capability of the Rotation Algorithm to estimate the displacement at any point along the height of a structure as well as the accuracy of the wireless sensors. From the figure, we can observe that the maximum gap between the estimate and true displacement is less than 1 mm.

5. Conclusions

In this paper, we propose a structural displacement estimation algorithm that utilizes the three-dimensional acclerometer and gyroscope. This algorithm has low computational complexity and can be embedded on wireless sensors. This advantage allows us to assess the structual health immediately after earthquakes. We discussed how to estimate the dynamic and residual displacements and validated the proposed algorithm using an experimental data set. Although the dynamic displacement estimation does not match the true measurement perfectly, the peak displacement is very similar to the true measurement. Besides, the esitmated residual displacement is alsomst identitical to the true measurement. Therefore, the proposed algorithm can provide a good indicator of the structral health evaluation.

6. Acknowledgements

We would like to thank the researchers involved with the experiments, Dr. Chia-Ming Chang and Dr. Shu-Hsieng Chow from NCREE, and graduate students Wei-Ting Hsu, Chun-Kai Chan, Tzu-Yun Hung and Sheng-Fu Chen from National Taiwan University (NTU) for their overall help and collaboration. Special thanks to Shieh-Kung Huang from NTU for his efforts on the experiment organization and coordination. We also thank the personnel of the NCREE for their help and accommodation. This research is partially supported by the NSF-NEESR Grant 1207911 and their support is gratefully acknowledged. The first author would like to thank the Charles H. Leavell Graduate Student Fellowship for the financial support.

6. References

[1] Celebi M, Sanli A (2002): GPS in pioneering dynamic monitoring of long period structures. *Earthquake Spectra*, 18(1), 47-61.

[2] Qian Z, Fan Y, Lu Z (2006): Application of draw-wire displacement sensors on structural health monitoring of jiangyin bridge. *SPIE Nondestructive Evaluation for Health Monitoring and Diagnostics*, 617619-617619.

[3] Sung S, Park J, Nagayama T, Jung H (2013): A multi-scale sensing and diagnosis system combing accelerometers and gyroscopes for bridge health monitoring. *Smart Materials and Structures*, 23(1), 015005.

[4] Wu Z, Li S (2007): Two-level damage detection strategy based on modal parameters from distributed dynamic macro-strain measurements. *Journal of Intelligent Material Systems and Structures*, 18(7), 667-676.

[5] Paulay T, Priestly M (1992): Principles of member design. *Seismic design of reinforced concrete and masonry buildings*, 95-157.

[6] Phan V, Saiidi MS, Anderson J, Ghasemi H (2007): Near-fault ground motion effects on reinforced concrete bridge columns. *Journal of Structural Engineering*, 133(7), 982-989.

[7] Cheung A, Kiremidjian AS (2014): Development of a rotation algorithm for earthquake damage diagnosis. *Earthquake Spectra*, 30(4), 1381-1401.

[8] Balafas K, Kiremidjian AS (2013): Extension of the rotation algorithm for earthquake damage estimation of complex structures. *SPIE Smart Structures and Materials + Nondestructive Evaluation and Health Monitoring*, 86920S-86920S.

[9] Polastre J, Szewczyk R, Cullr D (2005): Telos: enabling ultra-low power wireless research. *IEEE 4th International Symposium on Information Processing in Sensor Networks*, 364-369.

[10] Moteiv (2006): Tmote sky datasheet. *Online*, http://www.eecs.harvard.edu/~konrad/projects/shimmer/references/tmote-sky-datasheet.pdf .

[11] InvenSense (2013): MPU-6000 and MPU-6050 product specification revision 3.4. *Online*, http://store.invensense.com/datasheets/invensense/MPU-6050_DataSheet_v3%204.pdf.

[12] Liao Y, Mollineaux M, Hus R, Bartlett R, Singla A, Raja A, Bajwa R, Rajagopal R, Snowfort: an open source wireless sensor network for data analytics in infrastructure and environmental monitoring, *IEEE Sensors Journal*, 14(12), 4253-4263.